Available online at www.sciencedirect.com
SCIENCE DIRECT®
PERGAMON
Polyhedron 22 (2003) 2027–2038
POLYHEDRON
www.elsevier.com/locate/poly

Hybrid DFT study of electronic structure on quasi-one-dimensional halogen-bridged binuclear metal complexes (MMX)

Shuhei Nakano *, Yasutaka Kitagawa, Takashi Kawakami, Kizashi Yamaguchi

Department of Chemistry, Graduate School of Science, Osaka University, Toyonaka, Osaka 560-0043, Japan

Received 6 October 2002; accepted 27 January 2003

Abstract

The electronic structure of quasi-one-dimensional halogen-bridged binuclear metal complex $Ni_2(dta)_4I$ ($dta = CH_3CS_2^-$) was investigated by hybrid density functional theory. UB3LYP was successfully applied to reproduce averaged-valence spin density wave state. The magnetic interactions between Ni dimers were estimated by calculating effective exchange integrals (J_{ab}) using $Ni_2(dta)_4I$ dimer and tetramer models. Calculated J values were consistent with that of experimental results. The natural orbital analysis of the broken-symmetry UB3LYP solution were performed to elucidate symmetry-adapted molecular orbitals and their occupation numbers. Several chemical indices such as polyradical character and information entropy were introduced on the basis of the occupation numbers to discuss the bonding character of MMX chain. All these indices supports that $Ni_2(dta)_4I$ was in the strongly correlating electron system.

Keywords: Hybrid density functional theory; MMX; $Ni_2(dta)_4I$; Effective exchange interaction

1. Introduction

The quasi-one-dimensional halogen-bridged binuclear metal complex (so-called MMX chain) has been attracted much interest in terms of physical and chemical properties such as strong antiferromagnetism, metallic conductivity, various valence structure caused by 5+ formal charge on MM dimer (M = Ni, Pd, Pt), etc. Generally, this formal charge has been expected to distribute as follows;

a) AV(SDW)–X–$M^{2.5+}$–$M^{2.5+}$–X–$M^{2.5+}$–$M^{2.5+}$–X–
b) CDW–X–M^{2+}–M^{2+}–X–M^{3+}–M^{3+}–X–
c) CP–X–M^{2+}–M^{3+}–X–M^{2+}–M^{3+}–X–
d) ACP(SP)–X–M^{2+}–M^{3+}–X–M^{3+}–M^{2+}–X–.

The charge distribution pattern (a) is averaged-valence (AV) spin density wave (SDW) state, (b) is charge density wave (CDW) state, (c) is charge-polarization (CP) state, and (d) is alternate-charge-polarization (ACP) state or spin-Peierls (SP) state, respectively. Many studies surrounding electronic structure of MMX compounds have been performed experimentally [1–12]. For example, the X-ray diffraction experiment demonstrated that $K_4[Pt_2(pop)_4Br]\cdot 3H_2O$ ($pop = P_2O_5H_2^{2-}$) lies in the CDW state [2], whereas the Raman spectra showed that $Li_4[Pt_2(pop)_4I]4H_2O$ is in the AV (SDW) state [8]. The optical absorption experiments suggested the CP phase for $\{CH_3(CH_2)_7NH_2\}_4[Pt_2(pop)_4I]$ and the ACP phase for $Pt_2(dta)_4I$ ($dta = CH_3CS_2^-$) at a low temperature (< 80 K) [9]. Thus electronic structures of Pt_2 complexes are sensitive to ligand fields and bond alternation.

While in case of Ni complexes such as $Ni_2(dta)_4I$, bridging halogen were considered to be located at the midpoint of Ni dimers because of a large on-site Coulomb U. Wada et al. suggested the pattern (a) Mott–Hubbard insulator state by investigation of conductivity, X-ray spectrum, and reflection spectrum [6]. Kitagawa et al. also suggested (a) state from ^{129}I Mössbauer spectrum study [7]. Therefore, as for $Ni_2(dta)_4I$ complex, it has been thought to be (a) Mott–Hubbard insulating state. However, they proposed the

* Corresponding author. Tel.: +81-6-6850-5405; fax: +81-6-6850-5550.
E-mail address: snaka@chem.sci.osaka-u.ac.jp (S. Nakano).

0277-5387/03/$ - see front matter © 2003 Published by Elsevier Science Ltd.
doi:10.1016/S0277-5387(03)00250-X

new electronic structure by the study of Raman spectrum and magnetic susceptibility [10], in their recent works. They suggested the existence of α-, β-, γ-phase in $Ni_2(dta)_4I$ complex. Each phase showed $J_{ab} = -44$, 0, -470 K, respectively [11]. Moreover, from the investigation of magnetic susceptibility, α- and β-phase showed the field-induced phase transition [11]. Considering this new study, electronic structure of $Ni_2(dta)_4I$ has not been elucidated clearly yet. Thus investigation of MMX especially $Ni_2(dta)_4I$ complex is attractive work.

In this study, we examined AV electronic structure of $Ni_2(dta)_4I$ complex without halogen distortion following X-ray spectrum study [1]. First of all, the extended Hubbard–Peierls model [13–15] for MMX chains is introduced to characterize AV (SDW), CDW, CP and ACP states. The several hybrid DFT (HDFT) calculations have been carried out for cluster models of $Ni_2(dta)_4I$ to elucidate effective exchange integrals (J_{ab}) between spins on the Ni–Ni dimers. The calculated J_{ab} values have been compared with the experimental results to examine appropriate computational methods. The natural orbital (NO) analysis of the broken-symmetry (BS) HDFT solutions has been performed to determine symmetry-adapted (SA) molecular orbitals (MO) and their occupation numbers (n_i). These MO and n_i values are used to determine several chemical indices such as polyradical character and information entropy as in the case of CASSCF calculations which are hardly appreciable to large transition metal complexes.

2. Theoretical background

2.1. Hubbard–Peierls model

The electronic structures of MMX chains are sensitive to electron correlation effect and bond alternation. The orbital energy level of the p_z-orbital of halogen atom (X) usually lies lower than that of the d_z2-orbital of transition metal (M). Therefore, a one-dimensional dimerized 3/4-filled system (MMX) is reliably described by the Hubbard–Peierls model Hamiltonian [16–18] as

$$\begin{aligned} H = & -\sum_{i,\sigma}^{N} t_{\mathrm{MM}}(c^{\dagger}_{a,i,\sigma}c_{b,i,\sigma} + \mathrm{hc}) \\ & - \sum_{i=1,\sigma}^{N}[t_{\mathrm{MXM}} - \alpha(y_{b,i} + y_{a,i+1})](c^{\dagger}_{a,i+1,\sigma}c_{b,i,\sigma} + \mathrm{hc}) \\ & - \beta\sum_{i}^{N}(y_{a,i}n_{a,i} + y_{b,i}n_{b,i}) \\ & + U_{\mathrm{eff}}\sum_{i=1}^{N}(n_{a,i,\uparrow}n_{a,i,\downarrow} + n_{b,i,\uparrow}n_{b,i,\downarrow}) \end{aligned} \quad (1)$$

where $c^{\dagger}_{a,i,\sigma}$ (or $c^{\dagger}_{b,i,\sigma}$) creates an electron with spin σ at site a (or b) in the i-th dimer, and $n_{p,i,\sigma}$ ($p = a$, b) denotes the number density; $n_{p,i,\sigma} = c^{\dagger}_{p,i,\sigma}c_{p,i,\sigma}$. Concerning with the bond alternation (Peierls instability), $y_{a,i}$ means the displacement ($y_{a,i} = R_{a,i} - R_0$) of the M_a–X distance ($R_{\mathrm{Ma-X}}$) from its standard length (R_0) in the undistorted phase, and a change in the interdimer distance is given by ($y_{b,i} + y_{a,i+1}$). The t_{MM} and t_{MXM} are the intra- and inter-dimer transfer integrals, respectively. The interdimer transfer integral through the p_z(X)-orbital is assumed to change with the interdimer distance in the linear manner with coefficient α. The d_z2-orbital level is variable with the change of the M–X bond length with coefficient β. U_{eff} is the effective Coulomb repulsion integral ($U_{\mathrm{eff}} = U_{\mathrm{M}} - V_{\mathrm{MM}}$) given by the on-site ($U_{\mathrm{M}}$) and intrasite ($V_{\mathrm{MM}}$) Coulomb repulsion integrals.

The Hubbard–Peierls model can be used to depict qualitative orbital energy diagrams of the AV, CDW, CP and ACP states as illustrated in Fig. 1. In the AV state, the d_z2-orbitals with the same orbital energy interact to form the half filled dσ* orbital of the MM unit, and an unpaired electron or hole in the dσ* is delocalized over the unit to provide the averaged-valence (2.5+) charge density. On the other hand, the d_z2-orbital energy levels become shallow and deep depending on the distortion of halogen atom X from the center of the MXM bond. Therefore the valencies of the metal ions with shorter and longer M–X bonds become 3+ and 2+, respectively. The CDW, CP and ACP states are easily understood on the basis of these

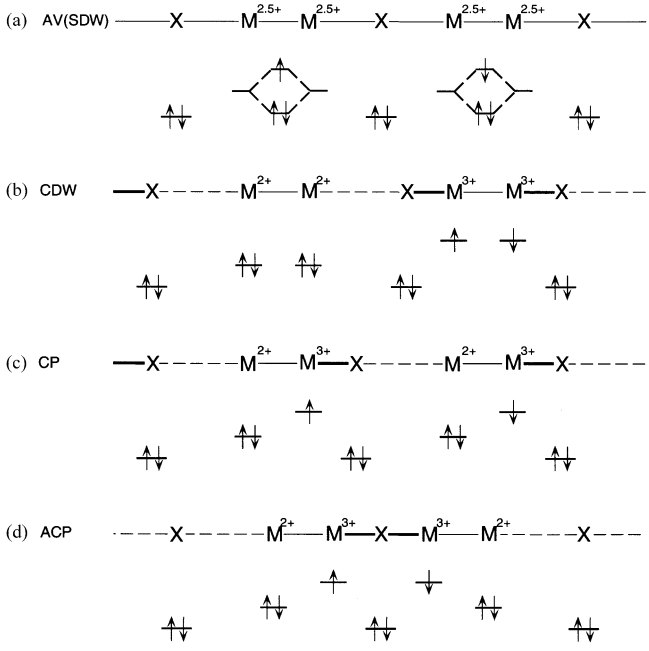

Fig. 1. The schematic illustrations of MMX chain with formal charge and corresponding orbital diagrams. The bold and broken lines show shorter and longer bond, respectively, and solid line indicates the undistorted bond.

energy levels as shown in Fig. 1. However, the electron–electron (e–e) interaction (U_{eff}) plays a crucial role for realization of four different electronic states. Recent numerical calculations [19] of the Hubbard–Peierls model have shown the phase diagrams: (a) AV SDW in the region; $U_{\text{eff}} \gg 0$, (b) CDW in the region; $U_{\text{eff}} \approx 0$, (c) CP in the region; $U_{\text{eff}} > 0$, $\alpha > 0$, $\beta \gg 0$. Therefore realization of these phases is highly depending on the parameters employed. However, the first principle calculations of them is not easy as shown later.

2.2. Heisenberg model

The effective exchange integrals between the unpaired electrons on the HOMO in the AV state in Fig. 1 are usually described by the Heisenberg model

$$\mathbf{H} = -2\sum J_{pq}\mathbf{S}_p\mathbf{S}_q \tag{2}$$

where J_{pq} is the effective exchange integral and $\mathbf{S}_r$ ($r = p, q$) is the spin operater at site r (r-th HOMO). The J_{pq} value is given by the perturbation method as

$$J_{pq} = -\frac{2t_{\text{MXM}}^2}{U_{\text{eff}}} \tag{3}$$

where t_{MXM} and U_{eff} are defined in the Hubbard–Peierls model in Eq. (1). The magnitude of $|J_{pq}|$ is sensitive to the transfer integral via the halogen (X) bridge, together with the effective Coulomb integral on the transition metal ion. Therefore J_{pq} value is one of the most appropriate parameters to check the reliability of the first principle calculation of MMX chain.

There are three different computational schemes of J_{pq} values by using the BS hybrid density functional methods as follows:

$$J_{ab}^{(1)} = \frac{{}^{\text{LS}}E_{\text{X}} - {}^{\text{HS}}E_{\text{X}}}{S_{\text{max}}^2} \tag{4a}$$

$$J_{ab}^{(2)} = \frac{{}^{\text{LS}}E_{\text{X}} - {}^{\text{HS}}E_{\text{X}}}{S_{\text{max}}(S_{\text{max}}+1)} \tag{4b}$$

$$J_{ab}^{(3)} = \frac{{}^{\text{LS}}E_{\text{X}} - {}^{\text{HS}}E_{\text{X}}}{{}^{\text{HS}}\langle S^2\rangle_{\text{X}} - {}^{\text{LS}}\langle S^2\rangle_{\text{X}}} \tag{4c}$$

where ${}^{\text{Y}}E_{\text{X}}$ and ${}^{\text{Y}}\langle S^2\rangle_{\text{X}}$ denote the total energy and total angular momentum of the spin state Y by method X (X = UHF, UDFT), respectively. S_{max} is the spin size of the high spin state. The first scheme $J_{ab}^{(1)}$ has been derived by Ginsberg [20], Noodleman and Davidson [21] (GND), while the second scheme $J_{ab}^{(2)}$ has been proposed by GND, Bencini, Ruiz (BR) and co-workers [22,23]. The third $J_{ab}^{(2)}$ scheme is our approximate spin-projected (AP) scheme. As shown previously, our $J_{ab}^{(3)}$ value [24–27] reduce to the $J_{ab}^{(1)}$ value by GND at the strong correlation limit ($x = |t_{\text{MXM}}|/U_{\text{eff}} \approx 0$), whereas it is equivalent to the $J_{ab}^{(2)}$ value at the weak correlation limit ($x = |t_{\text{MXM}}|/U_{\text{eff}} \gg 0$). Since the $J_{ab}^{(3)}$ scheme works well in the whole region ($0 < x < 1$), comparisons of $J_{ab}^{(1)}$, $J_{ab}^{(2)}$ and $J_{ab}^{(3)}$ values are effective to diagnose the strength of electron correlation effect in the MMX chain.

2.3. Derivation of J-value for $Ni_2(dta)_4I$

In this section, let us derive J-value for $Ni_2(dta)_4I$ dimer (**1**) and tetramer model (**2**) in Fig. 2(B) using Heisenberg model. In case of **1**, there are two spin sites. Thus J-value with and without spin projection at strong correlation region were expressed as Eqs. (4c) and (4a), respectively.

On the other hand, there are four spin sites in **2**. Thus we started from Eq. (2) to estimate spin unprojected J values. Fig. 3 illustrates the several magnetic interaction between spin sites. Using the Eq. (2), the energy of **2** was expressed as

$$E = -2(J_{ab}S_aS_b + J_{ac}S_aS_c + J_{ad}S_aS_d + J_{bc}S_bS_c + J_{bd}S_bS_d + J_{cd}S_cS_d) \tag{5}$$

where S_p ($p = a, b, c, d$) denotes the spin magnitude. When **2** has $(a, b, c, d) = (\uparrow, \downarrow, \uparrow, \downarrow)$ spin alignment, Eq. (5) becomes

$${}^{(a)}E = \frac{1}{2}J_{bc} + J_{ab} - J_{ac} + \frac{1}{2}J_{ad} \tag{6a}$$

Similarly, the energy of highest spin, other low spin, and intermediate spin states are expressed as

$(a, b, c, d) = (\uparrow, \uparrow, \uparrow, \uparrow)$:

$${}^{(b)}E = -\frac{1}{2}J_{bc} - J_{ab} - J_{ac} - \frac{1}{2}J_{ad} \tag{6b}$$

$(a, b, c, d) = (\uparrow, \downarrow, \downarrow, \uparrow)$:

$${}^{(c)}E = -\frac{1}{2}J_{bc} + J_{ab} + J_{ac} - \frac{1}{2}J_{ad} \tag{6c}$$

$(a, b, c, d) = (\uparrow, \uparrow, \downarrow, \downarrow)$:

$${}^{(d)}E = \frac{1}{2}J_{bc} - J_{ab} + J_{ac} + \frac{1}{2}J_{ad} \tag{6d}$$

$(a, b, c, d) = (\uparrow, \uparrow, \uparrow, \downarrow)$:

$${}^{(e)}E = -\frac{1}{2}J_{bc} + \frac{1}{2}J_{ad} \tag{6e}$$

From Eqs. (6a), (6b), (6c) and (6d), we simply obtained,

$$J_{ab} = \frac{{}^{(a)}E - {}^{(d)}E + {}^{(c)}E - {}^{(b)}E}{4} \tag{7}$$

$$J_{ac} = \frac{{}^{(c)}E - {}^{(b)}E - {}^{(a)}E - {}^{(d)}E}{4} \tag{8}$$

Substituting ${}^{(e)}E$ from ${}^{(a)}E$ and ${}^{(b)}E$, we obtained

$${}^{(a)}E - {}^{(e)}E = J_{bc} + J_{ab} - J_{ac} \tag{9}$$

$${}^{(b)}E - {}^{(e)}E = -J_{ab} - J_{ac} - J_{ad} \tag{10}$$

Adding $-J_{ab} + J_{ac}$ to Eq. (7) and $J_{ab} + J_{ac}$ to Eq. (8),

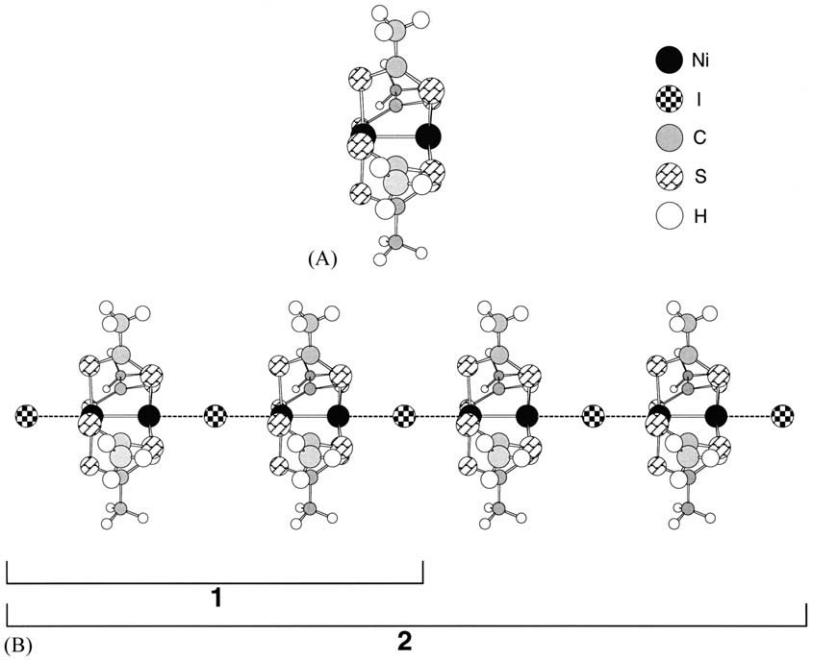

Fig. 2. The structure of (A) $Ni_2(dta)_4$, (B) $Ni_2(dta)_4I$ dimer (**1**) and tetramer model (**2**). The bond distance between C and H of methyl was set to be 1.09 Å.

we obtain J_{bc} and $-J_{ad}$, respectively. Thus five spin states as Eqs. (6a), (6b), (6c), (6d) and (6e) are necessary to estimate J value for **2**. This procedure was used in section 4.2.

3. Introduction of chemical indices

The SA CASCI or CASSCF calculations are desirable for systems where there are strong competitions between degenerate states. Such calculations are, however, difficult for large systems. In this case, NO analysis of BS UHF or UDFT can be an alternative method to obtain SA MO. These spin-polarized BS orbitals are expressed as follows;

$$\psi_i^+ = \cos\theta\phi_i + \sin\theta\phi_i^* \tag{11a}$$

$$\psi_i^- = \cos\theta\phi_i - \sin\theta\phi_i^* \tag{11b}$$

where θ is the orbital mixing parameter, and ϕ_i, ϕ_i^* are bonding- and antibonding- SA MOs, respectively. The up spins enter ψ_i^+ and down spins enter ψ_i^-. The orbital overlap $T_i = \langle\psi_i^+|\psi_i^-\rangle$ between the split orbitals i under the UHF or DFT approximations are written as

$$T_i = \langle\psi_i^+|\psi_i^-\rangle = \cos 2\theta \tag{12}$$

The NOs (SA MOs) and their occupation numbers [28] of UHF or UDFT solutions are determined by diagonalizing the first order density matrices. The occupation numbers are expressed with the orbital overlap T_i as follows;

$$n_{\mathrm{HOMO}-i}(\mathrm{W}) = 1 + T_i \quad \text{and} \quad n_{\mathrm{LUMO}+i}(\mathrm{W}) = 1 - T_i \quad (i = 0, 1, 2, \ldots) \tag{13}$$

where W = UHF or DFT. However, because of spin contaminations, the occupation number are different from those of spin-SA methods such as Perfect-Paring (PP) GVB, although the T_i value itself is usually close to the GVB value [28]. Then occupation numbers in PP-type spin projected UHF or UDFT solutions are derived to obtain the spin adapted values [29,30] as

$$n_{\mathrm{HOMO}-i}(\mathrm{PW}) = [n_{\mathrm{HOMO}-i}(\mathrm{W})]^2/(1 + T_i^2) \tag{14}$$

$$n_{\mathrm{LUMO}+i}(\mathrm{PW}) = [n_{\mathrm{LUMO}+i}(\mathrm{W})]^2/(1 + T_i^2) \tag{15}$$

where PW = PUHF or PDFT. Using the occupation numbers obtained by the NO analysis of BS solutions, we can define several chemical indices [31]. The SA CASCI and CASSCF calculations are not necessary for qualitative purpose.

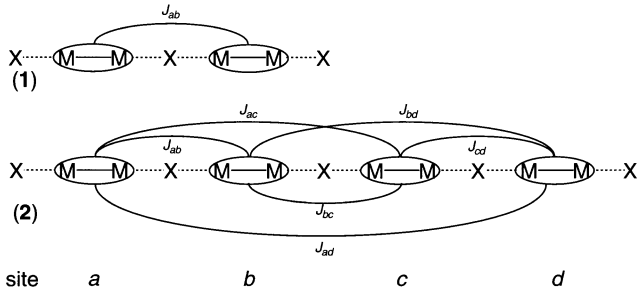

Fig. 3. The schematic illustrations of magnetic interactions. During the derivation in Section 2.3, we assumed $J_{ab} = J_{cd}$ and $J_{ac} = J_{bd}$ associated from it's symmetry.

Unpaired electron density T is introduced to express the deviation of any wavefunction from the single Slater determinant [30], and it can be expressed by the occupation numbers as

$$T_i = n_i(2 - n_i) \tag{16}$$

For the extension of T-value toward polyradical species ($2N$ electron system) [31], it is rewritten as

$$\tilde{T}_n = \frac{\sum_{i=1}^{2N} n_i(2 - n_i)}{2N} \tag{17}$$

where $2N$ is the maximum number at the strong correlation limit. As shown previously, $\tilde{T}_n$ value is responsible for electron localization or Coulomb hole between opposite spins [32].

Information entropy I is also introduced to express the chemical bond. The Jaynes information entropy [33–36] is defined by the occupation numbers as

$$I_i = -\sum_{i=1}^{N} n_i \ln n_i \tag{18}$$

and the normalized information entropy $\tilde{I}_n$ for $2N$ electron system [31] is defined as

$$\tilde{I}_n = \frac{2N \ln 2 - \sum_{i=1}^{N} n_i \ln n_i}{2N \ln 2} \tag{19}$$

where the maximum Jaynes (negative) entropy is given by $-2N \ln 2$ for the closed shell bonds. This normalized information entropy is a useful index to understand the kinetic energy correlation [35,36] in complex systems.

Lastly diradical character Y_i is introduced to express the contribution of doubly excited configuration (W_d) involved in the projected BS solution in comparison with CASSCF [28,29] as

$$Y_i = 2W_d = 1 - \frac{2T_i}{1 + T_i^2} \tag{20}$$

where T_i is orbital overlap defined by Eq. (13). This index is also extended to $2N$ electron system [31] as follows;

$$\tilde{Y}_n = \frac{1}{N} \sum_{i=1}^{N} \frac{(1 - T_i)^2}{1 + T_i^2} \tag{21}$$

where N is responsible for completely polyradical state ($T_i = 0$, $i = 1 - N$). This index is useful to diagnose the appropriate method of computation [37,38]. If chemical bond is in the strongly spin polarized region (region III), $\tilde{Y}_n$-value becomes almost 100%, while in non-magnetic region (region I), this value get closer to 0%. UHF and pure DFT are appropriate for region III and I, respectively. On the other hand, magnetic interaction in the intermediate region (region II) is well expressed by HDFT.

All chemical indices introduced here are related each other through the occupation number of NOs which can be calculated by BS solutions instead of SA CASSCF. This procedure is applicable to large systems for which the CASSCF are not feasible.

4. Computational details

The calculations were performed by the use of following basis sets; (i) Wachters+f basis set for Ni, and 6-31 1+G* basis set for C, S, H and 6-311G* for I, (ii) Wachters+f basis set for Ni, and 6-31+G* basis set for S, 6-31G for C and H, 6-311G* for I. The coordination was according to the x-ray measurement study [1]. Because this experimental data does not include the coordinates of hydrogen atoms on methyl of dta, they were estimated by the calculation of energy optimization at UB3LYP/4-31G level for $CH_3CS_2^-$ molecule. The calculated model were dimer and tetramer of $Ni_2(dta)_4I$. The above basis sets (i) was used for dimer model and (ii) was used for tetramer model. There were almost no differences between two basis sets except for Mulliken charge population, however, basis set (ii) could decrease computational costs. These calculation were performed using GAUSSIAN-98 program code [39].

5. Results

5.1. The electronic structure of $Ni_2(dta)_4$ complex

Before the calculation about MMX complex, we examined the MM complex. Since MMXs are oxidized compound from chain axis by halogen, investigation of electronic structure of MM is the first step to study MMX. The coordination of $Ni_2(dta)_4$ was taken from the study by Bellitto et al. [1] (Fig. 2(A)). In order to determine the ground state electron structure of

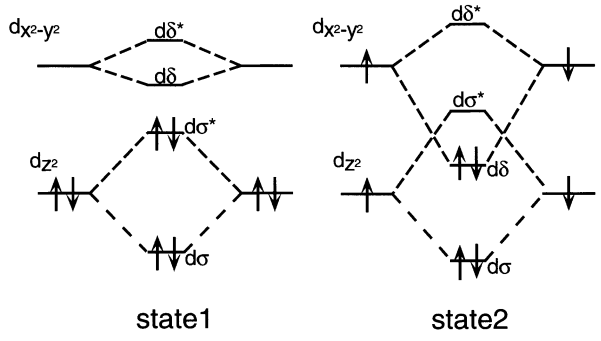

Fig. 4. MO correlation diagrams of the Ni–Ni dimer. State 1 and 2 indicate the closed-shell and high spin triplet structures for the Ni(II) ions, respectively.

$Ni_2(dta)_4$, we examined two possible electron structures in terms of Ni–Ni dimer (Fig. 4). The state 1 has empty $d\delta_{x^2-y^2}$ orbital constructed from low-spin Ni^{2+}, while the state 2 has half filled $d\sigma$ and $d\delta_{x^2-y^2}$ orbitals constructed from high-spin Ni^{2+}. The state 2 is possible electronic structure when energy level of $d\sigma$ competes with that of $d\delta_{x^2-y^2}$, which is familiar to octahedral complex. These calculations were performed for $Ni_2(dta)_4$ one unit but with ligand model using basis set (*i*). This one unit model is reasonable since $Ni_2(dta)_4$ has no one dimensional alignment and/or interaction such as MMX. Their results were listed in Table 1 in the form of relative energy difference from the state 1 on each method. Although generally $Ni_2(dta)_4$ has been considered to take state 1, Hartree–Fock (HF) estimated that state 2 become most stable, because in case of HF, dynamical electron correlation for the different spin was ignored. Therefore in order to consider electron correlation effect, second order Møller–Plesset perturbation theory (MP2) which can take dynamical correlation into account was performed. MP2 estimated that state 1 was more stable than state 2. The MP2 result is also reproduced by the HDFT methods such as B3LYP and B2LYP. Therefore we concluded that electron structure of Ni dimer in $Ni_2(dta)_4$ was state 1.

5.2. *J* value of AV (SDW) electron structure of $Ni_2(dta)_4I$ complex

Since $Ni_2(dta)_4I$ chain is an insulator, its cluster models give us various information which is advantageous to study electronic structures, since MO and DFT calculation gives us clear picture of electronic structure, such as orbital occupation, orbital energy, spin density, etc. In previous section, we determined the electronic structure of $Ni_2(dta)_4$, i.e. without oxidization of halogen from chain axis. The electron configuration on metal dimer was $(\sigma)^2\,(\delta_{xy})^2\,(\delta^*_{xy})^2\,(\pi)^4\,(\pi^*)^4\,(\sigma^*)^2$. Thus after the oxidization, simply we could assume $(\sigma)^2\,(\delta_{xy})^2\,(\delta^*_{xy})^2\,(\pi)^4\,(\pi^*)^4\,(\pi^*)^1$ configuration, namely σ^* orbital on one MM unit takes a role of one spin site. In order to examine AV electron structure, it was necessary to consider more than two spin sites. Thus two spin sites model (**1**) and four spin sites model (**2**) structures (Fig. 2) were examined using the basis sets (i) and (ii), respectively.

Table 1
The relative energy difference between state 1 and 2 calculated by HF, MP, and HDFT

	HF	MP2	B3LYP	B2LYP
State 1	0.00	0.00	0.00	0.00
State 2	−1.80	+2.22	+2.82	+1.07

As we mentioned before, SA CASCI or CASSCF calculations are desirable. Such calculations are, however, difficult for large clusters such as **1** and **2**. Since considering with four electrons from ligands and three electrons from σ and σ^* orbitals on Ni–Ni dimer, seven electrons in seven orbitals, CAS{7,7} is at least necessary, but not enough, for one MM unit. For **1** and **2** require at least CAS{14,14} and CAS{28,28}, respectively, these SA multiconfigurational calculations are not practicable. Instead of these treatments, spin-projection procedure for spin-polarized HDFT can be an alternative way for the investigation of magnetic interaction of system [38]. If there are two spin sites like **1**, J_{ab} value can be represented by Eq. (4c). While if system has more than two spin sites and in region II, we have considered an approximate but size-consistent spin-projection procedure [31,37], where the denominator of Eq. (4c) is modified as follows;

$$\Delta(ZII) = {}^{HS}\langle S^2\rangle(Z) - {}^{LS}\langle S^2\rangle(Z) - S_a g(N)[{}^{LS}\langle S^2\rangle(Z) - S_r(S_r+1)] \quad (22)$$

where

$$g(n) = (N-2)^2/N \quad (N>2 \text{ and even numbers}),\quad = (N-3) \quad (N>3 \text{ and odd numbers}) \quad (23)$$

and Z indicates methods such as UMP, UCC, DFT. S_r denotes the exact spin angular momentum for the clusters under the discussion:

$$S_r = n(S_a - S_b) \quad (N=2n),\quad = n(S_a - S_b) + S_a \quad (N=2n+1) \quad (24)$$

The effective exchange integral by the approximate spin-projected method Z are, therefore, given by

$$J_{ab}(AP-Z) = [{}^{LS}E(Z) - {}^{HS}E(Z)]/\Delta(ZII) \quad (25)$$

Using HDFT, UB3LYP, the AV electron structure was successfully obtained in both **1** and **2**. These calculated results were illustrated in Fig. 5. Judging from the spin densities, the electronic structure of **1** showed slightly inclined spin density to outer Ni atoms. This edge effect which comes from the limitation of model structure was suppressed in the results of **2**, namely the spin densities on the site *b* and *c* of **2** were delocalized equally on each Ni–Ni dimers. Several J_{ab} values were estimated with and/or without spin projection procedure. These results were listed in Table 2. Comparing with J_{ab}(**1**) and J_{bc}(**2**) obtained from spin unprojected procedure, the edge effect was significant since these values should be equal essentially. On the other hand, comparing with J_{ab}(**2**) and J_{bc}(**2**), although J_{ab}(**2**) was suffered from edge effect more or less, this error can be mitigated ($\sim$60 K). This tendency indicated that AV (SDW) state was stabilized due to the long range interaction. This long range interaction was

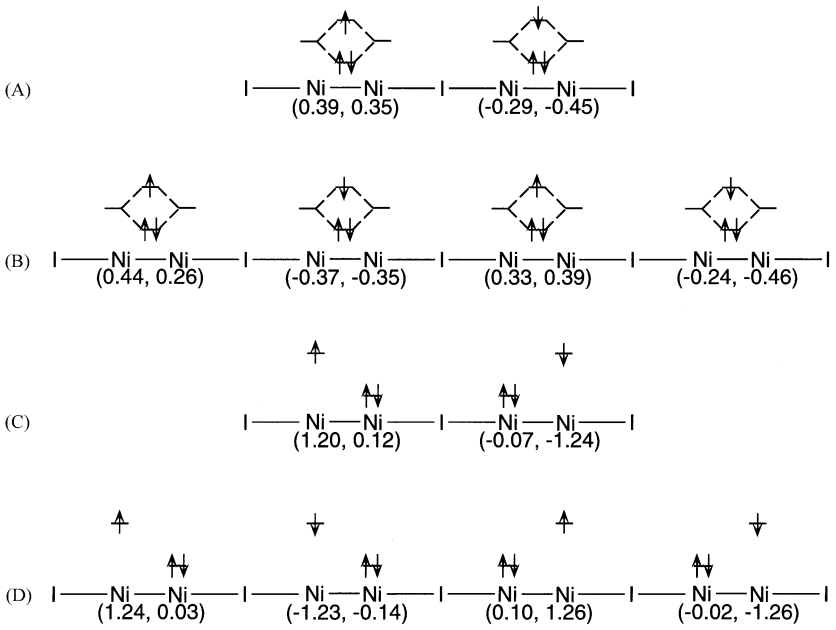

Fig. 5. (A) and (C) show the spin structure of Ni calculated by UB3LYP and UB2LYP using **1**, respectively. Similarly, (B) and (D) show spin structures for **2**. The number in parenthesis means the spin density of corresponding Ni atom.

evident from $J_{ac}(\mathbf{2})$ which still showed the antiferromagnetic interaction. In case of $J_{ad}(\mathbf{2})$, the sign became positive because the edge effect outweigh the magnetic interaction. Since $J_{ab}(\mathbf{2})$ and $J_{bc}(\mathbf{2})$ were almost equal, approximate spin projection procedure (Eq. (25)) was available. Suppose $J_{ab}(\mathbf{2}) \approx J_{bc}(\mathbf{2}) = J(\mathbf{2})$, $J(\mathbf{2})$ becomes -308 K. Comparing with the experimental results, these calculated results were consistent with the observed J value of γ phase.

There are nine σ-symmetry orbitals around HOMO and LUMO of **2** for each α and β spin orbitals which are constructed from dσ* of Ni–Ni and pσ of iodine. Fig. 6 illustrates BS orbitals (Kohn–Sham orbital) of **2** calculated by UB3LYP. The orbitals one and two were next LUMO and LUMO, respectively. Note that the orbital three was not HOMO. The six orbitals between two and three were omitted in this figure since they were mainly constructed from terminal iodine p-orbitals (i.e. p_x, p_y, p_z, of two terminal iodine) including two σ-symmetry orbitals. Similarly, six orbitals between three and four were constructed from nonbonding p-orbital (p_x, p_y) of bridging three iodine and omitted in the figure. The three σ-type orbitals three, four, and five were illustrated in order of orbital energy from the top of occupied orbital. The other lower two orbitals belonging to σ-type were omitted because of the limitation of space. Judging from these orbitals, following points were observed: (1) the unoccupied orbitals 1 and 2 depict hole orbitals. They were delocalized equally on Ni–Ni dimer. This indicated that hole or electron was delocalized on each Ni–Ni dimer (i.e. AV electron state). (2) These holes were strongly localized on each Ni–Ni dimer. This indicates the SDW type spin alignment. (3) The occupied σ-type orbitals were hybridized and broadly distributed at Ni–Ni dimer and iodine. This indicated that energy level of dσ* and pσ were in close range. (4) The orbital shape of pσ of iodine was so large. Thus it strengthened the super-exchange interaction between electron spin on Ni–Ni dimer. (5) δ-type orbitals which were in the next higher orbital of 1 were nearly degenerate with LUMO. This implies that in case of CASCI or CASSCF calculations, not only σ-type orbitals but also δ-type orbitals should be considered as active space.

Table 2
J value [a] without and with approximate spin projection calculated by UB3LYP [b]

Spin unprojected scheme					AP-scheme	
1	**2**				**1**	**2**
J_{ab}	J_{bc}	J_{ab}	J_{ac}	J_{ad}	J	J
−597	−368	−305	−19	+22	−580	−308

[a] K.
[b] J_{bc} (**2**) value denotes J value calculated for 2 using UB3LYP in the text.

5.3. Obtained electronic structure by UB2LYP

In case of strongly correlated systems such as cuprate [40] or Cr acetate [41], traditional DFT often fail to estimate J values. UB2LYP can be appropriate functional in such cases. This functional was also examined for $Ni_2(dta)_4I$, since Ni related halogen-bridged metal complexes such as $Ni(chxn)_2X_3$ (chxn = 1R,2R-cyclo-

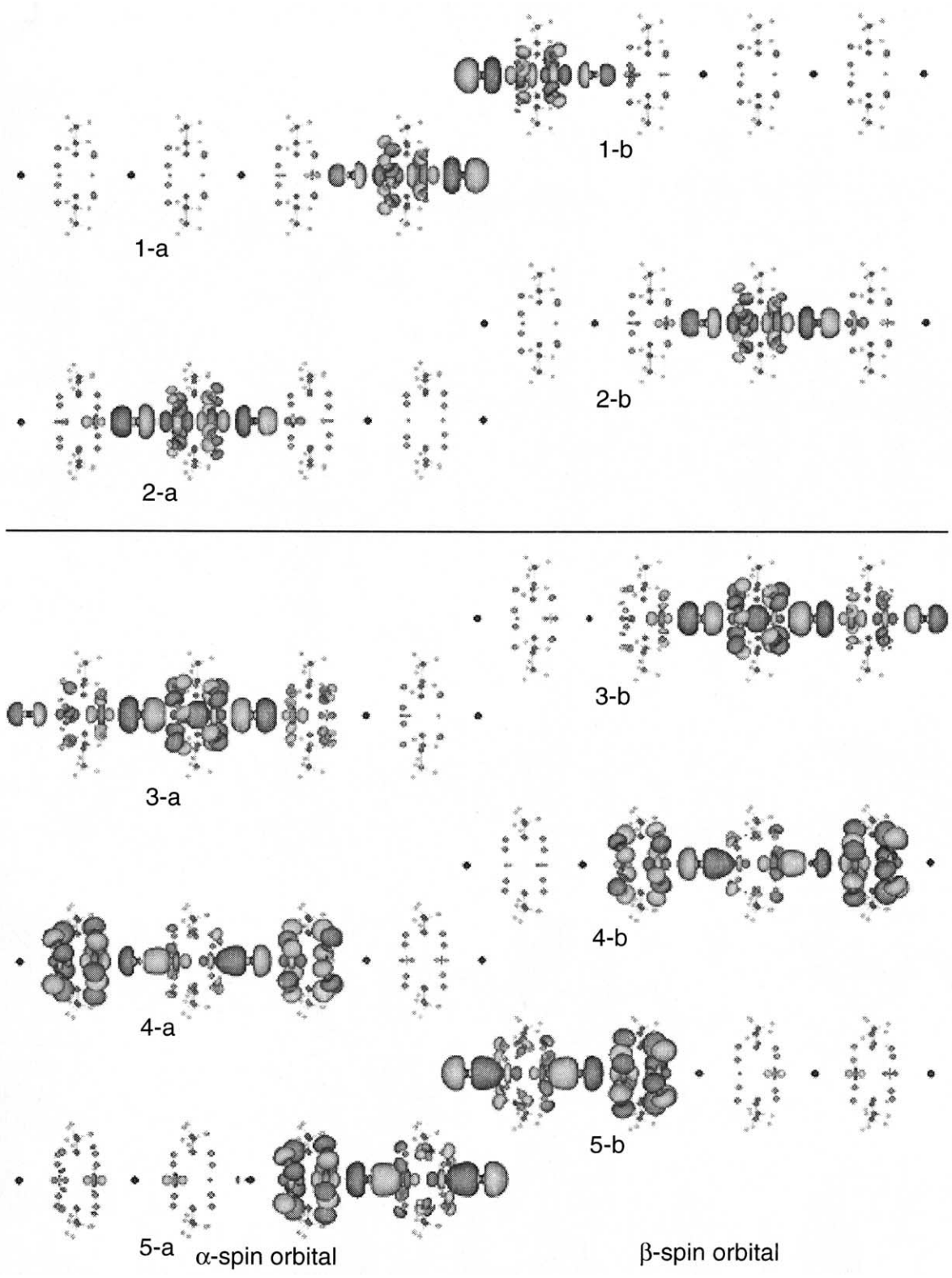

Fig. 6. The σ-type broken symmetry orbitals for **2** by UB3LYP. 1c ($c = a, b$) were unoccupied orbitals, while 4c, 5c and 6c were occupied orbitals.

hexanediamine, X = Cl, Br) [42] are considered to be strongly correlated systems. The calculated models were **1** and **2** as same as previous section. The obtained electronic structures were illustrated in Fig. 5. Unlike the results by UB3LYP, UB2LYP failed to reproduce AV state. The electron spin ($S = 1/2$) was localized on outer Ni atom of Ni–Ni dimer. This tendency was observed in both **1** and **2**. Thus the difference between

the results of UB3LYP and that of UB2LYP was the description of electron spin on Ni–Ni dimer. These results indicated that UB2LYP overestimated the on-site Coulomb repulsion U on the Ni–Ni dimer, and this overestimation prevented an electron spin delocalizing on Ni–Ni dimer with soft ligands ($CH_3CS_2^-$). Therefore we concluded that in order to describe AV electron structure by DFT, UB3LYP is proper functional judging from the spin density populations.

5.4. Natural orbitals and chemical indices

In this section, we investigated $Ni_2(dta)_4I$ complex from the view points of NO and several chemical indices: $\tilde{T}_n$, $\tilde{I}_n$, and $\tilde{Y}_n$ using **2**. The first order density matrices obtained by UB3LYP were diagonalized to obtain the NOs and their occupation numbers. Fig. 7 illustrates NOs (namely, SA MOs) of σ-symmetry, and occupation numbers are listed in Table 3. Since these occupation numbers were obtained by BS solutions, they also suffer from spin contamination. Then the occupation numbers in spin projected UB3LYP were derived using Eqs. (14) and (15) and listed in Table 3. Judging from these occupation numbers (n_i(PUB3LYP)), the occupation number of HOMO and LUMO were still near 1 and that of next HOMO was near 1.5. This implies that spin polarization effect, more exactly electron correlation effect, is obviously serious but not so strong as complete polyradical.

Calculated $\tilde{T}_n$ value was 94%. This means that electron or Coulomb hole was localized on each Ni–Ni unit, that is, there were large U on Ni–Ni unit. $\tilde{I}_n$ value of this system was 82%. This normalized information entropy can express the degree of spin coupling. If system is in completely spin-coupled electron state, this index should be 0%. While it is in completely spin-polarized state, this will be 100%. The calculated result indicates more or less spin-polarized state. When we discuss the spin-Peierls electron state, further discussion about the relationship between $\tilde{I}_n$ value and inter-unit distances seems to be necessary. Calculated $\tilde{Y}_n$ value was 59%. This indicates that the strength of correlation effect is intermediate, suggesting the utility of UB3LYP method. On the other hand, UB2LYP results in overestimation of U or underestimation of resonance effect on Ni–Ni dimer since it is categorized as HDFT for much more strongly correlated systems.

Table 3
The occupation number, spin-projected occupation number, normalized unpaired electron density, normalized information entropy, and normalized polyradical character calculated [a] by UB3LYP

	n_I	n_i(P)	$\tilde{T}_n$	$\tilde{I}_n$	$\tilde{Y}_n$
NLUMO [b]	0.67	0.41			
LUMO	0.88	0.76			
HOMO	1.12	1.24			
NHOMO	1.33	1.59			
			0.94	0.82	0.59

[a] The notations are given in text.
[b] N means the next orbital.

6. Discussion and concluding remarks

6.1. The electron structure of $Ni_2(dta)_4I$

According to the experimental study, $Ni_2(dta)_4I$ is considered to be semiconductor [6]. This character was well described by UB3LYP calculation which estimated the energy gap between 4a and 3a orbitals in Fig. 6 was 1.79 eV. Considering these results and obtained J value, calculated electron structure was consistent with experimental results (γ-phase of $Ni_2(dta)_4I$). As shown previously [43], UB3LYP can describe semiconducting or metallic behavior. On the other hand, UB2LYP can describe insulating state such as copper oxide. The calculated results indicated that AV (SDW) electron structure was obtained by UB3LYP not UB2LYP. This implies that there was not so large U on Ni–Ni dimer as copper oxide [40], and considering resonance effect between Ni atoms in Ni–Ni dimer was significant. This is why not UB2LYP but UB3LYP could describe AV (SDW) electron structure.

The resonance effect and U were discussed about intra-dimer so far. Here, we discuss the ratio of inter-dimer transfer energy and U_{eff} x in Section 2.2 defines this ratio ($|t_{\mathrm{MXM}}|/U_{\mathrm{eff}}$) and is expressed as orbital overlap [31] as follows;

$$\tilde{T}_i = \frac{\sum_i^N T_i}{N} = 2x \tag{26}$$

where T_i is defined by Eq. (13) and $\tilde{T}_i$ is normalized orbital overlap. Then x was obtained as 0.113. From Eq. (3), U_{eff} and t_{MXM} were estimated as 1.03 and 0.116 eV respectively. All these calculated results supports that $Ni_2(dta)_4I$ is in the strongly correlated system.

Table 4
J value (cm^{-1}) calculated for the naked Cr(II) dimer (Cr_2^{4+}) by AP-UB3LYP [a], AP-UB2LYP, UNOCASCI [a] and CASSCF [a]

R/Å	AP-UB3LYP	AP-UB2LYP	UNOCASCI{8,8}	CASSCF{8,8}
2.000	−1249	−918.2	−805.9	−832.6
2.015	−1191	−875.0	−752.3	−776.2
2.389	−369.3	−275.2	−156.2	−158.2
2.500	−260.6	−196.5	−100.5	−101.5
3.000	−56.63	−45.62	−13.00	−13.07

[a] Ref. [44].

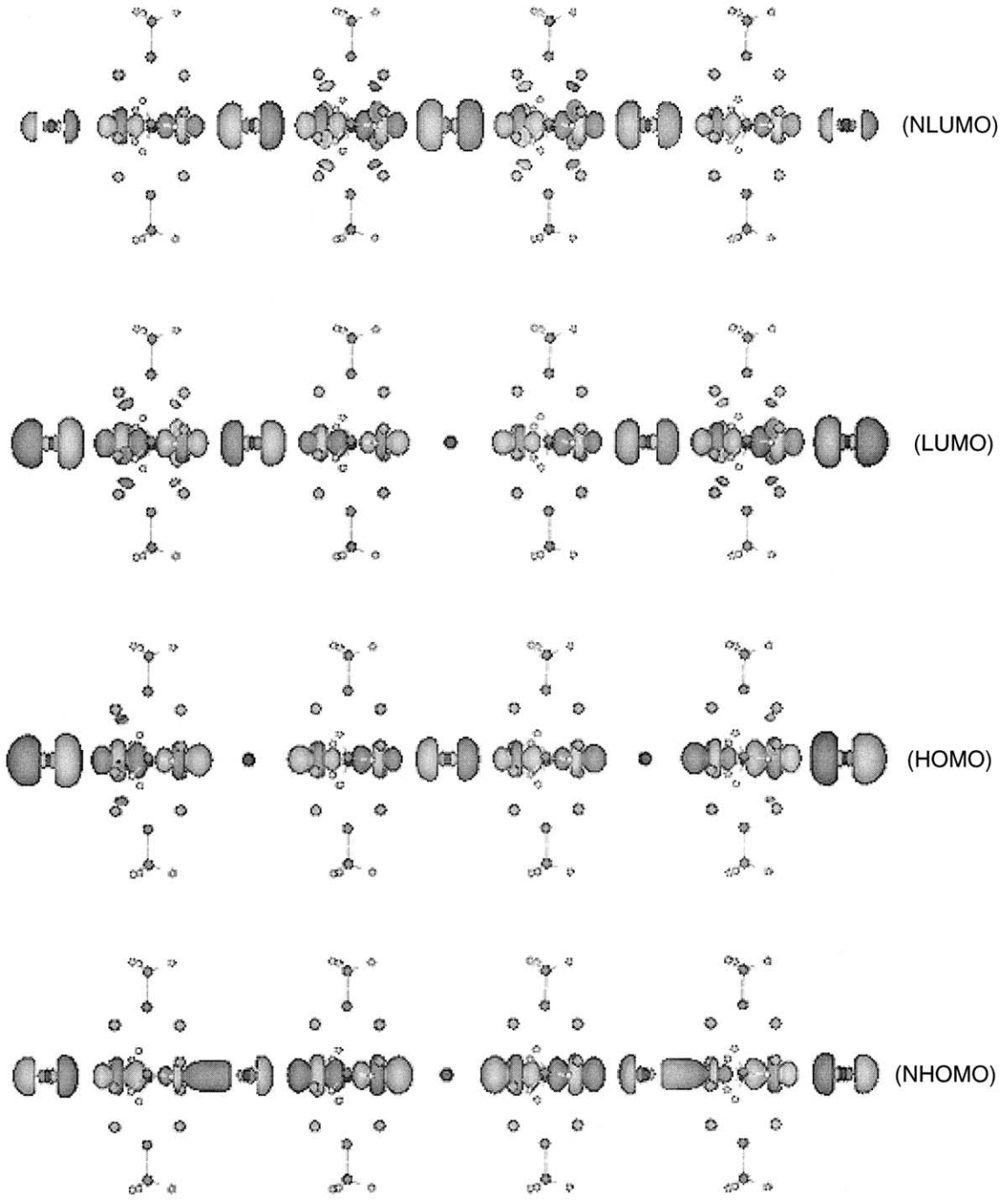

Fig. 7. MO obtained by the natural orbital analysis of the UB3LYP solution. The occupation numbers are given in Table 3.

Table 5
J value (cm^{-1}) between Cr and Ni using HDFT and CAS calculations

System	mS2VWN	UNOCASCI{5,5}	CASSCF{5,5}	CASPT2{5,5}	UNOCASCI{9,9}	Exp.
Cr(III)CNNi(II)	49.9 [a]	1.312	1.256	4.373	1.501	
$(NC)_5$ Cr(III)CNNi(II)$(CN)_5$	15.61					16.8 [b]

[a] Ref. [46].
[b] Ref. [47].

6.2. CASCI, CASSCF, CASPT2, and BS-DFT

As we mentioned before, SA CASCI or CASSCF calculations are desirable. It is, however, impracticable for large calculation target like **2**. For such cases, BS-DFT can be alternative approach to estimate magnetic interaction. There are some evidences: (1) The J value of several binuclear Cr(II) model were calculated in Ref. [44]. They were compared with the results by DFT. These results indicated that DFT can be utilized for computations of J value for larger system instead of UNOCASCI and CASSCF. Table 4 listed the obtained J value calculated by AP-UB3LYP, AP-UB2LYP, CASCI and CASSCF. The conventional UB3LYP overestimated the $|J|$ value for the Cr(II)–Cr(II) bond, while UB2LYP could reproduce J value calculated by CAS calculations. (2) J value for Cr(III)–CN–Ni(II) was calculated [45] by the CASCI, CASSCF, CASPT2, and BS-HDFT. In case of Cr(III)–CN–Ni(II) model calculations, there are clear difference between J value by CAS calculations and that by BS-DFT. It is well-known that adding ligands suppresses J value. Thus J value of $(NC)_5Cr(III)–CN–Ni(II)(CN)_5$ calculated by mS2VWN became 15.61 cm^{-1} (Table 5). This value was quite consistent with experimental value. On the other hand, estimated J value by CASPT2 calculations were about 4 cm^{-1}. Considering with ligands effect, J value will be less than 4 cm^{-1} for $(NC)_5Cr(III)–CN–Ni(II)(CN)_5$. This means that very larger CAS space than [5,5] is necessary for CASPT2. Therefore BS-DFT can be powerfull and practicable tools instead of SA-CAS calculations for the estimation of magnetic interactions of large systems.

6.3. Concluding remarks

The HDFT and its approximately spin projected version were performed for $Ni_2(dta)_4I$ to estimate magnetic interactions. UB3LYP could successfully applied to reproduce AV (SDW) electron structure. Obtained J values were consistent with that of γ-phase of $Ni_2(dta)_4I$. The NO analysis of the UB3LYP solutions were performed to obtain SA MOs and their occupation numbers. Several chemical indices defined by using them were introduced to discuss the bonding character of the system. All obtained results supported that $Ni_2(dta)_4I$ was strongly correlated system. Comparing these indices with those of other complexes such as $Pt_2(dta)_4I$ are now in progress to examine various electron structure from the view points of chemical indices. The crystal orbital calculations of these systems are also in progress.

Acknowledgements

This work has been supported by a Grant-in-Aid for Scientific Research on Priority Areas (Nos. 14204061 and 13740396) from Ministry of Education, Culture, Sports, Science and Technology, Japan.

References

[1] C. Bellitto, G. Dessy, V. Fares, Inorg. Chem. 24 (1985) 2815.
[2] M. Yamashita, K. Toriumi, Inorg. Chim. Acta. 178 (1990) 143.
[3] M. Yamashita, Y. Wada, K. Toriumi, T. Mitani, Mol. Cryst. Liq. Cryst. 216 (1992) 207.
[4] Y. Wada, M. Yamashita, Proceedings of the First International Conference on Intelligent Materials, 147 (1992).
[5] T. Mitami, Y. Wada, M. Yamashita, K. Toriumi, A. Kobayashi, H. Kobayashi, Synth. Met. 64 (1994) 291.
[6] Y. Wada, T. Furuta, M. Yamashita, K. Toriumi, Synth. Met. 70 (1995) 1195.
[7] H. Kitagawa, T. Sonoyama, T. Mitani, M. Seto, Y. Maeda, Synth. Met. 103 (1999) 2159.
[8] M. Yamashita, S. Miya, T. Kawashima, T. Manabe, T. Sonoyama, H. Kitagawa, T. Mitani, H. Okamoto, R. Ikeda, J. Am. Chem. Soc. 121 (1999) 2321.
[9] H. Kitagawa, N. Onodera, T. Sonoyama, M. Yamamoto, M. Fukawa, T. Mitani, M. Seto, Y. Maeda, J. Am. Chem. Soc. 121 (1999) 10068.
[10] R. Makiura, H. Kitagawa, R. Ikeda, Mol. Cryst. Liq. Cryst. 379 (2002) 309.
[11] H. Kitagawa, R. Makiura, R. Ikeda, Private communication.
[12] H. Okamoto, private communication.
[13] K. Nasu, J. Phys. Soc. Jpn. 52 (1983) 3865.
[14] K. Nasu, J. Phys. Soc. Jpn. 52 (1984) 302.
[15] K. Nasu, J. Phys. Soc. Jpn. 52 (1984) 427.
[16] J.T. Gammel, A. Saxena, I. Batistic, A.R. Bishop, S.R. Phillpot, Phys. Rev. B 45 (1992) 6408.
[17] K. Iwano, J. Phys. Soc. Jpn. 66 (1997) 1088.
[18] (a) S. Yamamoto, Phys. Lett. A 247 (1998) 422;
(b) S. Yamamoto, Phys. Lett. A 258 (1999) 183.
[19] M. Kuwabara, K. Yonemitsu, J. Phys. Soc. Jpn, in press.
[20] A.P. Ginsberg, J. Am. Chem. Soc. 102 (1980) 111.
[21] L. Noodleman, E.R. Davidson, Chem. Phys. 109 (1986) 131.
[22] A. Bencini, F. Totti, C.A. Doul, K. Doclo, P. Fantucci, V. Barone, Inorg. Chem. 36 (1997) 5022.
[23] E. Ruiz, J. Cano, S. Alvarez, P. Alemany, J. Comp. Chem. 20 (1999) 1391.
[24] K. Yamaguchi, Y. Takahara, T. Fueno, Applied Quantum Chemistry, (V.H. Smith et al., Eds.) Reidel, Boston, MA, 1986, p. 155.
[25] K. Yamaguchi, F. Jensen, A. Dorigo, K.N. Houk, Chem. Phys. Lett. 149 (1988) 537.
[26] T. Soda, Y. Kitagawa, T. Onishi, Y. Takano, Y. Shigeta, H. Nagao, Y. Yoshioka, K. Yamaguchi, Chem. Phys. Lett. 319 (2000) 223.
[27] Y. Takano, S. Kubo, T. Onishi, H. Isobe, Y. Yoshioka, K. Yamaguchi, Chem. Phys. Lett. 335 (2001) 395.
[28] K. Yamaguchi, in: R. Carbo, M. Klobukowski (Eds.), Self-Consistent Field Theory and Applications, Elsevier, Amsterdam, 1990, p. 727.
[29] K. Yamaguchi, Chem. Phys. Lett. 33 (1975) 330.
[30] K. Takatsuka, T. Fueno, K. Yamaguchi, Theor. Chim. Acta 48 (1978) 176.
[31] K. Yamaguchi, T. Kawakami, Y. Takano, Y. Kitagawa, Y. Yamashita, H. Fujita, Int. J. Quant. Chem. 90 (2002) 370.

[32] K. Yamaguchi, Chem. Phys. 25 (1977) 215.
[33] C.E. Shannon, Bell. Syst. Tech. 27 (1948) 379.
[34] E. Jaynes, in: R. Rosencrants (Ed.), Papers on Probability, Statics and Statical Physics, Reidel, Dordrecht, 1993.
[35] D.M. Collins, Z. Naturforsch 48A (1993) 68.
[36] J.C. Ramírez, C. Soriano, R.O. Esquivel, R.P. Sagar, M. Hô, V.H. Smith, Jr., Phys. Rev. A56 (1997) 4477.
[37] T. Kawakami, S. Yamanaka, Y. Takano, Y. Yoshioka, K. Yamaguchi, Bull. Chem. Soc. Jpn. 71 (1998) 2097.
[38] Y. Kitagawa, T. Soda, Y. Shigeta, S. Yamanaka, Y. Yoshioka, K. Yamaguchi, Int. J. Quant. Chem. 84 (2001) 592.
[39] GAUSSIAN-98, Revision A.11.3, M.J. Frisch, G.W. Trucks, H.B. Schlegel, G.E. Scuseria, M.A. Robb, J.R. Cheeseman, V.G. Zakrzewski, J.A. Montgomery, Jr., R.E. Stratmann, J.C. Burant, S. Dapprich, J.M. Millam, A.D. Daniels, K.N. Kudin, M.C. Strain, O. Farkas, J. Tomasi, V. Barone, M. Cossi, R. Cammi, B. Mennucci, C. Pomelli, C. Adamo, S. Clifford, J. Ochterski, G.A. Petersson, P.Y. Ayala, Q. Cui, K. Morokuma, N. Rega, P. Salvador, J.J. Dannenberg, D.K. Malick, A.D. Rabuck, K. Raghavachari, J.B. Foresman, J. Cioslowski, J.V. Ortiz, A.G. Baboul, B.B. Stefanov, G. Liu, A. Liashenko, P. Piskorz, I. Komaromi, R. Gomperts, R.L. Martin, D.J. Fox, T. Keith, M.A. Al-Laham, C.Y. Peng, A. Nanayakkara, M. Challacombe, P.M.W. Gill, B. Johnson, W. Chen, M.W. Wong, J.L. Andres, C. Gonzalez, M. Head-Gordon, E.S. Replogle, and J.A. Pople, Gaussian, Inc., Pittsburgh, PA, (2002).
[40] T. Onishi, Y. Takano, Y. Kitagawa, T. Kawakami, Y. Yoshioka, K. Yamaguchi, Polyhedron 20 (2001) 1177.
[41] Y. Kitagawa, T. Kawakami, Y. Yoshioka, K. Yamaguchi, Polyhedron 20 (2001) 1189.
[42] H. Okamoto, K. Toriumi, T. Mitani, M. Yamashita, Phys. Rev. B42 (1990) 10381.
[43] S. Nakano, Y. Kitagawa, T. Kawakami, K. Yamaguchi, Synth. Met., in press.
[44] M. Nishino, S. Yamanaka, Y. Yoshioka, K. Yamaguchi, J. Phys. Chem. A 101 (1997) 705.
[45] M. Nishino, Y. Kitagawa, K. Yamaguchi, Chem. Phys. Lett. 297 (1998) 51.
[46] M. Nishino, S. Kubo, Y. Yoshioka, A. Nakamura, K. Yamaguchi, Mol. Cryst. Liq. Cryst. 305 (1997) 109.
[47] T. Mallah, S. Ferlay, C. Auberger, C. Helary, F. L'Hermite, R. Ouahes, J. Vaissermann, M. Verdaguer, P. Veillet, Mol. Cryst. Liq. Cryst. 273 (1995) 141.